Astronomy & Astrophysics

Orbital and physical parameters of eclipsing binaries from the All-Sky Automated Survey catalogue

III. Two new low-mass systems with rapidly evolving spots

K. G. Hełminiak[1,2], M. Konacki[1,3], K. Złoczewski[4], M. Ratajczak[1], D. E. Reichart[5], K. M. Ivarsen[5], J. B. Haislip[5], J. A. Crain[5], A. C. Foster[5], M. C. Nysewander[5], and A. P. LaCluyze[5]

[1] Nicolaus Copernicus Astronomical Center, Department of Astrophysics, ul. Rabiańska 8, 87-100 Toruń, Poland
e-mail: xysiek@ncac.torun.pl
[2] Departamento de Astronomía y Astrofísica, Pontificia Universidad Católica, Vicuña Mackenna 4860, Casilla 306, Santiago 22, Chile
[3] Astronomical Observatory, Adam Mickiewicz University, ul. Słoneczna 36, 60-286 Poznań, Poland
[4] Nicolaus Copernicus Astronomical Center, ul. Bartycka 18, 00-716 Warszawa, Poland
[5] Department of Physics and Astronomy, University of North Carolina, Campus Boc 3255, Chapel Hill, NC 27599-3255, USA

ABSTRACT

Aims. We present the results of our spectroscopic and photometric analysis of two newly discovered low-mass detached eclipsing binaries found in the *All-Sky Automated Survey* (ASAS) catalogue: ASAS J093814-0104.4 and ASAS J212954-5620.1.

Methods. Using the Grating Instrument for Radiation Analysis with a Fibre-Fed Echelle (GIRAFFE) on the 1.9-m Radcliffe telescope at the South African Astronomical Observatory (SAAO) and the University College London Echelle Spectrograph (UCLES) on the 3.9-m Anglo-Australian Telescope, we obtained high-resolution spectra of both objects and derived their radial velocities (RVs) at various orbital phases. The RVs of both objects were measured with the two-dimensional cross-correlation technique (TODCOR) using synthetic template spectra as references. We also obtained *V* and *I* band photometry using the 1.0-m Elizabeth telescope at SAAO and the 0.4-m Panchromatic Robotic Optical Monitoring and Polarimetry Telescopes (PROMPT) located at the Cerro Tololo Inter-American Observatory (CTIO). The orbital and physical parameters of the systems were derived with PHOEBE and JKTEBOP codes. We compared our results with several sets of widely-used isochrones.

Results. Our multi-epoch photometric observations demonstrate that both objects show significant out-of-eclipse modulations, which vary in time. We believe that this effect is caused by stellar spots, which evolve on time scales of tens of days. For this reason, we constructed our models on the basis of photometric observations spanning short time scales (less than a month). Our modeling indicates that (1) ASAS J093814-0104.04 is a main sequence active system with nearly-twin components with masses of $M_1 = 0.771 \pm 0.033 \ M_\odot$, $M_2 = 0.768 \pm 0.021 \ M_\odot$ and radii of $R_1 = 0.772 \pm 0.012 \ R_\odot$ and $R_2 = 0.769 \pm 0.013 \ R_\odot$. (2) ASAS J212954-5620.1 is a main sequence active binary with component masses of $M_1 = 0.833 \pm 0.017 \ M_\odot$, $M_2 = 0.703 \pm 0.013 \ M_\odot$ and radii of $R_1 = 0.845 \pm 0.012 \ R_\odot$ and $R_2 = 0.718 \pm 0.017 \ R_\odot$.

Conclusions. Both systems seem to confirm the well-known characteristic of active low-mass stars, for which the observed radii are larger and the temperatures lower than predicted by evolutionary models. Other parameters agree within errors with the models of main sequence stars. The time-varying spot configuration may imply a variable level of activity, which may manifest itself in small changes of the measured radii.

Key words. binaries: eclipsing – binaries: spectroscopic – stars: fundamental parameters – stars: late-type – stars: individual: ASAS J093814-0104.4 – stars: individual: ASAS J212954-5620.1

1. Introduction

Since the discovery of the first eclipsing late-type systems – YY Gem (Kron 1952; Bopp 1974), CM Dra (Lacy 1977) or CU Cnc (Delfosse et al. 1999) – and the first comparisons of their observed properties with the evolutionary models (e.g. Lacy 1977), it became clear that the stellar evolution theory, despite being very successful in many fields, fails to reproduce the observed parameters of late-type stars, especially radii and temperatures. An increasing number of recently discovered systems (see Torres et al. 2010, for a recent review) confirms these discrepancies at least for systems on the main sequence. Predicted radii of low-mass stars are systematically larger and temperatures lower than the ones derived from observations. It is now claimed that this is caused by the improper treatment of stellar activity and convection in outer layers of the stellar interior. A presence of a close companion and its gravitational influence seems to increase the activity level and suppresses the effectiveness of convection. Considering that the amount of energy produced in the core is the same for single stars as for close binary components, this leads to larger radii and lower effective temperatures while at the same time keeping the overall luminosity at an unchanged level (Chabrier et al. 2007; Morales et al. 2009). However, in order to better constrain and understand these differences between models and observation, more low-mass systems showing various levels of activity and with accurately known parameters are needed.

In this paper we present the first analysis together with the orbital and physical parameters of two new spectroscopic detached eclipsing binaries (DEBs), both with component masses

below 1 $M_\odot$ – ASAS J093814-0104.4 (hereafter ASAS-09) and ASAS J212954-5620.1 (hereafter ASAS-21) – and both showing substantial level of activity. For ASAS-09 we reach 2.7–4.3% level of precision in the masses and ∼1.6% in radii. This is better or close to the level of 3 % required for stringent tests of the evolutionary models (Blake et al. 2008; Clausen et al. 2008). For ASAS-21 we reach ∼2.0% for masses and 1.4–2.4% for radii. Both systems were noticed to present significant out-of-eclipse and time-varying brightness modulations, which we deduce to be caused by spots and their evolution on the time scale of single weeks.

Both objects are be interesting from the evolutionary point of view. ASAS-09 is composed of two nearly identical dwarfs and iso be a good candidate for testing the so-called Vogt or Vogt-Russel theorem (Vogt 1926). ASAS-21 on the contrary shows one of the lowest (still quite high however) mass ratios measured in low-mass binaries – $q \sim 0.85$. The components of systems with low q lay relatively far from each other on the isochrones, which allows to perform more stringent tests of the stellar models than for systems with q close to 1.

2. ASAS-09 and ASAS-21

2.1. ASAS-09 (GSC 04894-02310)

The eclipsing binary ASAS J093814-0104.4 is the faintest of all low-mass detached eclipsing binaries in our sample of systems found in the ASAS catalogue and has $V = 12.07 \pm 0.12$ mag (Pojmański 2002). Its eclipsing nature was noted for the first time in the *ASAS Catalogue of Variable Stars*[1] (ACVS; Pojmański 2002). The system is classified in ACVS as an eclipsing detached binary (ED) with the amplitude of the photometric variation of 0.47 mag and $(V - I) = 1.12$ mag (Szczygieł et al. 2008). It can be associated with a soft X-ray source 1RXS J093813.2-010423 ($F_X = 0.40 \pm 0.06 \times 10^{-12}$ erg cm^{-2} s^{-1}, Voges et al. 1999)

The ASAS data phase coverage is full and the time span covers almost nine years but, the scatter reaches almost 0.4 mag not only due to the quality of the data but also due to the evolution of stellar spots on relatively short time scales. The ASAS light curve phase-folded with the orbital period from our analysis is presented in Fig. 1. It shows nearly equal eclipses and, not surprisingly, no clear out-of-eclipse variations.

2.2. ASAS-21 (GSC 08814-01026)

The eclipsing system ASAS J212954-5620.1 has an apparent V magnitude of 11.83 ± 0.10 (Pojmański 2002). The first information about its variability or binarity can be found in the ACVS, where this system is classified as ED with the amplitude of the photometric variation of 0.77 mag and $(V - I) = 1.29$. It also has a soft X-ray identification – 1RXS J212954.0-561954 ($F_X = 0.714 \pm 0.102 \times 10^{-12}$ erg cm^{-2} s^{-1}).

As for the previous system, the available ASAS photometry spans about nine years and covers the entire orbit. The ASAS curve phase-folded with the period obtained from our modeling is shown in Fig. 1. One can see a considerable difference in the depths of eclipses and hints of an out-of-eclipse variation. The photometric scatter is increased by the evolution of the spots as well.

3. Observations

3.1. Spectroscopy

ASAS-09 and ASAS-21 were observed spectroscopically as candidate late-type detached eclipsing binaries (DEBs) in order to obtain their radial velocity (RV) curves and confirm their low masses. The latter system was observed earlier, at the very beginning of our survey, during four consecutive nights in June 2006. We used the SAAO's 1.9-m Radcliffe telescope and its Grating Instrument for Radiation Analysis with a Fibre-Fed Echelle (GIRAFFE) to obtain a series of $R \sim 40\,000$ spectra. Because of the faintness of the target we set the exposure time to 3600 s. The spectra were later binned four times in the dispersion direction in order to improve their low signal-to-noise ratio (SNR). In the best cases, we reached $SNR \sim 70$ per collapsed pixel in the center of an échelle order near $\lambda = 6500$ Å. This value varied with weather conditions (seeing). The wavelength calibration was done in the standard manner with the ThAr lamp exposures taken before and after a stellar exposure.

Two additional spectra of ASAS-21 were taken with the AAT/UCLES during our observing run in September 2008. We used a 1 arcsec slit, which provides a resolution of $R \sim 60\,000$. With 900 s exposures and no binning we reached a significantly lower $SNR \sim 25$, but a comparable RV precision of several km s^{-1}.

We observed ASAS-09 in January 2009 with the same configuration of the AAT/UCLES. Despite even lower SNR (∼15–20) we were able to derive RV measurements with a km s^{-1} precision. As in the case of Radcliffe/GIRAFFE data, the wavelength calibration was done in the standard manner with the ThAr lamp. An additional drawback during our Australian observations was a very poor seeing (typically well above 2 arcsec). However, we were still able to obtain useful data for the two objects.

The radial velocities for both systems were obtained in the same way as described in our previous papers – Hełminiak et al. (2009, hereafter Paper I) and Hełminiak & Konacki (2010, hereafter Paper II) – with the TODCOR technique (Zucker & Mazeh 1994) and the synthetic ATLAS spectra (Castelli & Kurucz 2003) as templates. The iodine cell available at AAT/UCLES was not used because of the low brightness of both targets. Owing to the low SNR and the rotational broadening, we did not perform any abundance analysis.

3.2. Photometry

Because ASAS-09 is a short period and a well detached system, it was considered as a low-mass candidate from the beginning of our survey. Thus it was observed photometrically well before the spectroscopic follow-up. We used the 1.0-m Elizabeth telescope at the South African Astronomical Observatory (SAAO) and a 1024×1024 STE4 camera with the Johnson V and Cousins I filters. The field of view was 317×317 arcsec (0.31 arcsec/pix) and the exposure time varied in order to compensate for varying observing conditions. The data were processed with the standard data reduction tasks available in the *IRAF* package[2].

Three separate data sets, covering both eclipses (without the secondary minimum) and their vast surroundings, were

---

[1] http://www.astrouw.edu.pl/asas/

[2] *IRAF* is written and supported by the *IRAF* programming group at the National Optical Astronomy Observatories (NOAO) in Tucson, AZ. NOAO is operated by the Association of Universities for Research in Astronomy (AURA), Inc. under cooperative agreement with the National Science Foundation. http://iraf.noao.edu/.
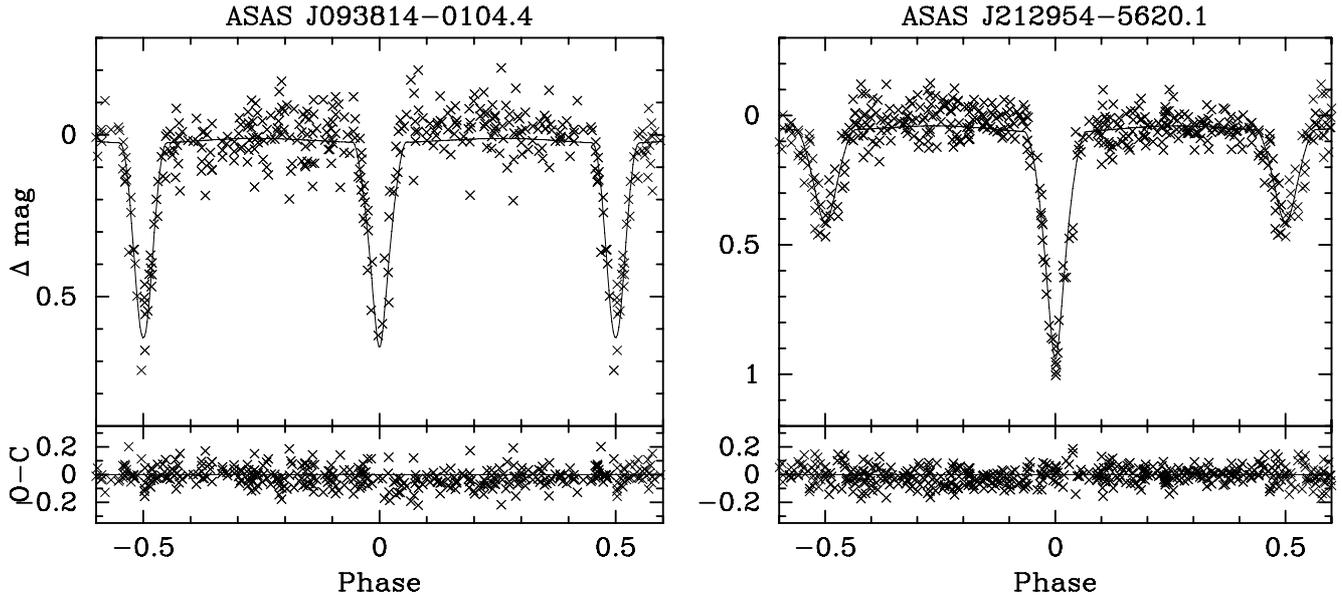
Fig. 1. ASAS *V* band light curves of ASAS-09 (*left*) and ASAS-21 (*right*) phase-folded with the best fitting orbital periods (see Table 3). Solid lines represent models based on our solutions (see Sect. 3.2) but without spots.

obtained in January 2008, December 2008, and March 2009. A clear out-of-eclipse modulation is seen, which originates in stellar spots. However, we failed to produce a final model of the system, because the data sets occurred to be inconsistent, which can be explained by an evolution of the spot pattern. Considering this, we decided to carry out additional observations using the Panchromatic Robotic Optical Monitoring and Polarimetry Telescopes (PROMPT).

PROMPT, located at CTIO in Chile, consists of six robotic 0.41-m Ritchey-Chrétien telescopes equipped with rapid-response Alta U47+ cameras and a wide range of astronomical filters. Telescopes serve mainly for taking rapid and simultaneous multi-wavelength observations of gamma-ray bursts (GRB) afterglows. PROMPT is operated by SKYNET – a distributed network of robotic telescopes located around the world, dedicated for continued GRB afterglow observations. For our purposes, we used Prompt-4 and Prompt-5 with Johnson's *V* and *I* filters and 1024×1024 cameras, giving 604×604 arcsec field of view (0.59 arcsec/pix). Our PROMPT observations of ASAS-09 took place in January 2010. We were able to obtain nearly full *V* and *I* light curves in two weeks. We consider this time scale as the limit for the time-consistency of the light curve.

ASAS-21 was observed at SAAO in May 2008 with the same instrumentation as ASAS-09. The partial light curve again shows a spot-originated out-of-eclipse variation. PROMPT observations carried out in June 2009 were initially performed in order to fill the gaps in the system's light curves but it immediately became clear that the new data show different light variations and that a consistent model cannot be constructed. In July 2009 we used PROMPT to obtain a new light curve, which covers all orbital phases. Owing to rapid spot evolution we could not use the June and July data together, since again we noticed substantial differences in the out-of-eclipse pattern (mainly near the secondary eclipse).

The last part of the data comes from SAAO observations taken in October 2009 and again shows a different light modulation. Because of challenging conditions, the moments of the minima were recorded only in the *V* band, we failed in our attempts to create a separate solution based on this data set alone.

Table 1. Number of photometric data points for each data set in the *V* and *I* bands for both systems.

	ASAS-09			ASAS-21	
Data set	*V* band	*I* band	Data set	*V* band	*I* band
2008-01	41	43	2008-05	166	164
2008-12	97	113	2009-06	127	159
2009-03	140	159	2009-07	120	120
2010-01	232	292	2009-10	129	118

The absolute calibration procedure for SAAO data, described in our Paper II, was based on the catalogue information of stars in the observed fields. For PROMPT we obtained additional observations of Landolt standard fields 53 ($\alpha = 06:52:12$, $\delta = -00:18:00$) and 54 ($\alpha = 06:52:31$, $\delta = -00:16:30$; Landolt 1992) with both telescopes (Prompt-4 and 5). The instrumental magnitudes of the standard stars were corrected for the atmospheric extinction and transformed in a traditional manner to the Johnson's system. In order to improve the calibration for SAAO we compared instrumental magnitudes of the stars common in SAAO and PROMPT fields of ASAS-09, ASAS-21 and three other systems observed by us with both instruments. Our final transformations result in the magnitudes' absolute uncertainties $\sigma_V = 0.013$ and $\sigma_I = 0.016$ mag in the *V* and *I* bands respectively. The total number of the data points collected in every data set for both binaries is shown in Table 1.

4. Analysis

4.1. Spectroscopic orbits

In the analysis of ASAS-09 and ASAS-21 we slightly modified our approach as presented in Papers I and II. We firstly took the ASAS light curve (nine year time span) and derived the orbital period P and T_0 with the fast and stable code JKTEBOP (Southworth et al. 2004a,b), based on EBOP (*Eclipsing Binary Orbit Program*, Popper & Etzel 1981; Etzel 1981). This step was especially necessary for the ASAS-09 system. We also inspected

Table 2. Barycentric radial velocities of ASAS-09 and ASAS-21.

Date (TDB) −2 450 000.0	v_1 km s^{-1}	±	O−C	v_2 km s^{-1}	±	O−C
ASAS-09						
From AAT/UCLES						
4837.1911	136.75	1.75	0.34	−93.08	4.99	−1.14
4837.2062	131.96	1.69	1.86	−87.62	4.52	−1.99
4840.1398	−57.14	1.95	−1.39	106.51	3.94	6.17
4840.2420	−100.56	2.21	1.17	141.33	4.75	−5.03
ASAS-21						
From Radcliffe/GIRAFFE						
3903.6543	−125.31	1.33	0.37	112.00	3.20	−0.53
3903.6949	−141.05	1.07	0.34	130.09	3.05	−1.08
3904.6314	32.74	2.48	2.12	−72.70	2.93	1.42
3905.5318	87.00	1.52	−1.20	−144.90	3.86	−3.72
3906.5668	−135.15	1.28	−1.30	123.63	2.35	4.69
3906.6109	−105.44	1.40	0.57	85.47	2.94	−0.03
3906.6489	−67.42	1.72	2.75	51.39	3.11	−4.11
From AAT/UCLES						
4727.0620	−97.72	1.61	−2.56	76.92	3.40	0.58
4728.0651	95.93	3.99	0.59	−148.10	2.05	1.15

Table 3. Spectroscopic orbital parameters of ASAS-09 and ASAS-21.

Parameter	ASAS-09 Value	±	ASAS-21 Value	±
P [d]	0.8974204	2.0e-6	0.7024303	3.0e-7
T_0 [JD-2 450 000]	5205.2949	3.0e-4	5009.86436	9.0e-5
K_1 [km s^{-1}]	126.9	1.3	126.4	1.0
K_2 [km s^{-1}]	127.4	2.7	149.7	1.4
γ_1 [km s^{-1}]	22.7	3.1	−16.6	0.6
$\gamma_2 - \gamma_1$ [km s^{-1}]	−0.3	2.5	1.7	2.8
q	0.996	0.023	0.844	0.011
$a \sin i$ [$R_\odot$]	4.510	0.052	3.834	0.023
e	0.0	(fix)	0.011	0.005
ω [°]	–	–	80.	30.
$M_1 \sin^3 i$ [$M_\odot$]	0.767	0.033	0.830	0.016
$M_2 \sin^3 i$ [$M_\odot$]	0.764	0.021	0.701	0.013

Notes. Values of P, T_0, e and ω for both systems are taken from the joined spectroscopic and photometric analysis performed with PHOEBE. ($\gamma_2 - \gamma_1$) was held fixed to 0 in the further analysis of both systems.

the ASAS light curves for hints of orbital eccentricity, but in both cases e was indistinguishable from 0 from the ASAS data only.

We used the values of P and T_0 to obtain a preliminary orbital solution using RV measurements independently of the light curve. We used a simple procedure, which fits a double-Keplerian orbit and minimizes the χ^2 function with a Levenberg-Marquardt algorithm. For ASAS-09 we kept the ephemeris and eccentricity fixed and fitted for the RV semi-amplitudes K_1 and K_2 and systemic velocities for the primary and secondary γ_1 and γ_2. For both systems we found $\gamma_1 - \gamma_2$ indistinguishable from 0, so we kept it fixed to 0 in the further analysis. For ASAS-21 we also set T_0, e and the periastron longitude ω free and fitted for them with $K_{1,2}$ and $\gamma_{1,2}$. We found e to have a small but significant value of 0.03 ± 0.02. It was later corrected to 0.011 ± 0.005 with the values and uncertainties of P, T_0 and ω based on the joined spectroscopic and photometric analysis performed with PHOEBE. After correcting the values of e, P, T_0, and ω, we ran our code again (keeping them fixed) to obtain final values of all spectroscopic parameters.

The formal RV measurement errors were computed from the bootstrap analysis of TODCOR maps created by adding randomly selected single-order TODCOR maps. For ASAS-09 the formal errors are underestimated. In order to obtain a reduced χ^2 of the best fit equal to ∼1, we added in quadrature an additional error, which was 0.85 and 3.70 km s^{-1} for the primary and secondary respectively. For ASAS-21 we reached a reduced χ^2 of the best fit close to 1, so no additional error was added to the ASAS-21 RV measurements. To compensate for the differences in the two spectrographs we shifted our RVs obtained with the AAT/UCLES for the this system by a constant value of -4.16 ± 2.90 km s^{-1}. This value probably originates in the intrinsic properties of the instruments and its uncertainty was included in the further analysis.

The velocities, their final errors, and O−Cs from the best-fitting model are collected in Table 2. The errors at the level of $1-5$ km s^{-1} are probably due to the low SNR, the rotational broadening, which reaches 44 km s^{-1} for ASAS-09 and 61 km s^{-1} for ASAS-21 (both systems seem to be tidally locked), template spectra mismatch, the activity and, of course, the systematic term (3.70 km s^{-1} for ASAS-09 secondary) probably originating in the activity itself. Still, the TODCOR maxima

were always well separated, hence blending of the spectral lines of the components did not affect the velocities.

In order to verify that the formal least-squares errors of the best fit parameters are correct, we carried out a bootstrap analysis. To this end we created 1000 artificial RV data sets by drawing replacement RVs from the original RV data sets and fitting the model for each such set. These best-fit parameters were then used to create the distribution for each model parameter and to compute the corresponding uncertainty. The bootstrap uncertainties were fully consistent with the ones from the formal least-squares fitting. This most likely means that the formal uncertainties are conservative even though the number of single RV datapoints – 8 for ASAS-09 and 18 for ASAS-21 – is relatively low. Additionally, we performed a Monte-Carlo simulation to estimate the systematic errors of derived parameters. The values of fixed parameters were randomly perturbed by values from a Gaussian distribution with σ equal to the given parameter error. The resulting systematic terms, even if they are at an order of magnitude smaller than the formal ones, were added in quadrature to the errors from the least-squares fit. We believe that this procedure ensures that the error values we obtained are well estimated, at least when not including the influence of the spots (see Sect. 5.4).

We present the derived spectroscopic parameters for both binaries in Table 3 and our best fitting models in Fig. 2. One should note that the RV semi-amplitudes of ASAS-09 differ by only 0.5 km s^{-1}, which is well within their errors. Thus we deal with a system composed of (nearly) twin stars. At present only three low-mass systems show this situation: YY Gem (Torres & Ribas 2002), BD −22 5866 (Shkolnik et al. 2008) and LP 133-373 (Vaccaro et al. 2007), with the last one having the largest uncertainty in the determination of masses. Two other low-mass binaries – GU Boo (Windmiller et al. 2010) and Tres-Her0-07621 (Creevey et al. 2005) – have their q consistent with 1 within 2σ. In the sample of 95 binary systems with their component masses and radii determined with accuracy better than 3%, presented by Torres et al. (2010), only 13 systems meet this criterium (including YY Gem).

ASAS-21 is on the opposite side of the mass-ratio distribution. According to Lucy (2006), there is a statistically significant narrow peak in the q distribution function for $q \gtrsim 0.95$ (the strong twin hypothesis). Halbwachs et al. (2003) also refer
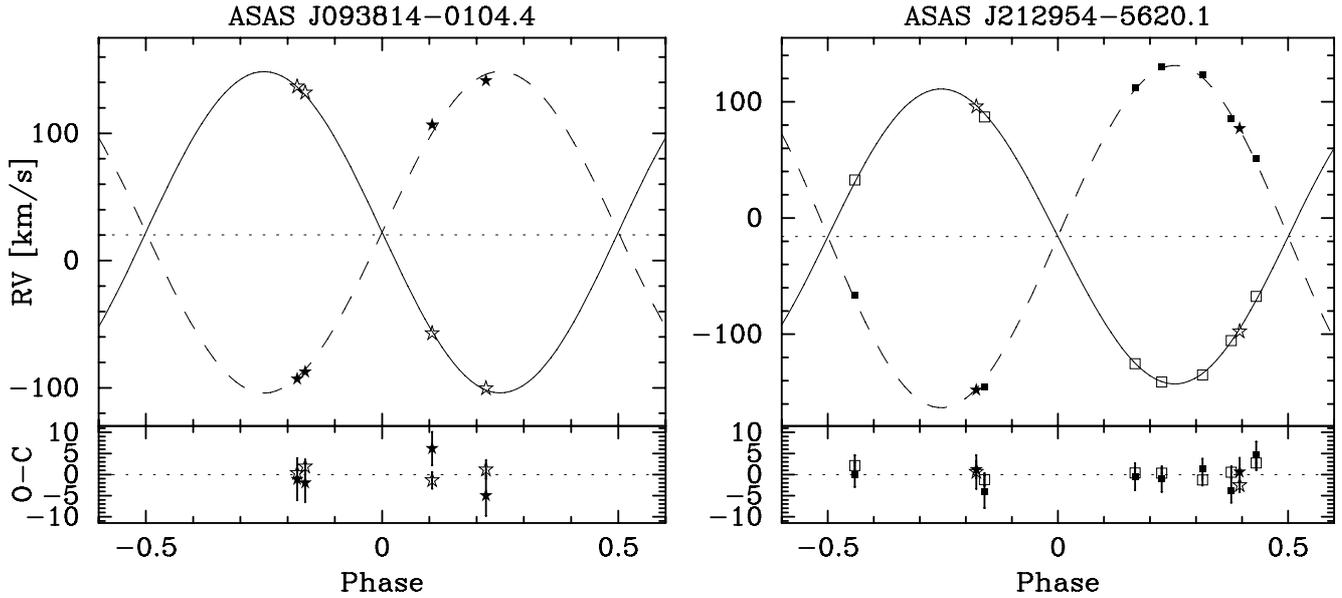
Fig. 2. Radial velocities of ASAS-09 (*left*) and ASAS-21 (*right*) from our AAT/UCLES (stars) and Radcliffe/GIRAFFE (squares) spectra together with the best fitting models. The measurements for the primaries are plotted with open and for the secondaries with filled symbols. The solid line shows the best fit for the primaries and the dashed line for the secondaries. The dotted line shows the systemic velocity γ.

to a broad peak for $q \gtrsim 0.85$, however this is still not confirmed. In the sample presented by Torres et al. (2010), 42% of systems have their $q \geq 0.95$ within errorbars, and 76% have $q \geq 0.85$. ASAS-21 is clearly far from the narrow peak and only marginally in the wide one. This makes it especially interesting for testing evolutionary models, because within the same absolute errorbars it is more difficult and constraining to fit a single isochrone to a low-q system than to a $q \sim 1$ system.

4.2. Spotted light curves

In order to obtain full and reliable models of our eclipsing binaries, we used time-consistent photometric data sets. For ASAS-09 we used only the PROMPT observations from January 2010 and created a single "base" model. For ASAS-21 we used the PROMPT data from July 2009 and created a family of models. We combined our RVs and V and I light curves with the *PHysics Of Eclipsing BinariEs* (PHOEBE; Prša & Zwitter 2005) code, which is an implementation of the Wilson-Devinney (WD) code (Wilson & Devinney 1971, with updates). It uses the computed gravitational potential of each star to calculate the surface gravity and effective temperatures and allows for adding several single spots on both components and fit for their size, position, and temperature. We used the square-root limb-darkening law (Diaz-Cordovez & Gimenez 1992) with the coefficients automatically interpolated by PHOEBE from the van Hamme LD tables (van Hamme 1993). The reflection albedos for both components were held fixed at the value of 0.5 as is appropriate for convective envelopes. The gravity brightening coefficient was set to 0.32 – the classical value obtained by Lucy (1967).

4.2.1. ASAS-09 – single "base" solution

While creating the "base" model of the ASAS-09 binary with PHOEBE, we followed our approach presented in Paper II. We firstly improved the ephemeris, then fitted for the temperatures, inclination, and potentials. Later we added a single, large cold spot on the secondary component (the one that is eclipsed

at $\phi = 0.5$) and "manually" fitted for its position, size, and temperature until the out-of-eclipse modulation was reproduced in a satisfactory way. Finally, we set free the spot parameters, the component temperatures and potentials, and the inclination angle. The initial solutions were obtained separately for PROMPT V and I curves combined with RVs. Because we found those initial results consistent, we used both the PROMPT light curves and RVs to create the final solution and reduce the parameter uncertainties.

The initial values of the temperatures were taken from the empirical color-temperature calibration by Casagrande et al. (2006) and both component colors were taken from PHOEBE, which enables one to compute separately the flux for every component in every band and also seems to keep the $V - I$ color at a stable level, independently from the given temperatures. In this way the final values of the temperatures should be consistent with those from the models and calibrations. Their uncertainties also include the absolute photometric calibration errors.

When deciding about the spot configuration, we wanted to keep the model as simple and robust as possible. The observed sine-wave modulation can be explained by a presence of only one large spot, which reaches across or covers the polar regions of the star. The choice of the component for the spot location was determined by the depth of the eclipses and the mass ratio. We found that if the spot was on the primary and thus was eclipsed at the phase $\phi = 0$ (close to the maximum of the spot's appearance), the effective temperature ratio of both components would then have to be substantially different from 1 in order to reproduce the observed eclipse depths. By placing the spot on the secondary, we keep the temperature ratio close to 1, which is expected for stars of nearly identical masses.

Before we established that a solution is the "base" one, we checked if it reproduced other light curves only by changing parameters of the spots. We also had to fit for the luminosity scaling factors, in order to account for small magnitude uncertainties which originate from the rms of the absolute photometric calibration. Using PHOEBE, we could force the luminosity levels to be decoupled from the temperatures, which we held fixed. In

Table 4. Absolute physical parameters adopted for ASAS-09.

ASAS-09	Primary		Secondary	
Parameter	Value	±	Value	±
inclination[°]		86.55 ± 0.20		
a [$R_\odot$]		4.519 ± 0.054		
Mass [$M_\odot$]	0.771	0.033	0.768	0.021
Ω-potential	6.866	0.040	6.887	0.040
Radius [$R_\odot$]	0.772	0.012	0.769	0.013
$\log g$	4.550	0.013	4.554	0.011
v_{synch} [km s^{-1}]	43.5	0.7	43.2	0.7
$V - I$ [mag]	1.170	0.13	1.172	0.13
T_{eff} [K]	4360	150	4360	150
M_{bol} [mag]	6.53	0.10	6.54	0.10
M_V [mag]	7.22	0.16	7.23	0.16
distance [pc]		151 ± 9		

this way we were able to reproduce other photometric data sets without changing any of the stellar parameters.

The parameters derived from the solution we adopted for ASAS-09 are presented in Table 4. From the PHOEBE solution we took the Ω-potentials, temperatures and inclination, and used them with the orbital parameters to derive the absolute masses, radii (thus $\log g$), luminosities (thus magnitudes), and the distance. In order to calculate them we used the procedure JKTABSDIM, which is available with JKTEBOP. The distance was calculated on the basis of derived M_{bol}, the observed magnitudes in several bands – ours V and I, and J, H, K_S from 2MASS (Cutri et al. 2003) – and various bolometric corrections (Bessel et al. 1998; Flower 1996; Girardi et al. 2002). The distance given in Table 4 is a weighted average of eight separately calculated results. We reached the best consistency between the results from various bands for $E(B-V) = 0$. As expected, our model predicts nearly equal values of all the parameters for both components.

The final models of the ASAS-09 system at various epochs are shown in Fig. 3. We present our observations and their respective models in the chronological sequence. For the January 2008 data, we did not apply any spots. The December 2008 solution involves a cold spot on the primary (not eclipsed) component. We reproduce the March 2009 data set by including in the model a bright spot (hotter than the surroundings) on the primary (eclipsed) component. In this way we can explain that the eclipse recorded in March 09 is deeper than that of January 2008. Bright spots were already used as an explanation for observed out-of-eclipse variations, for example in GU Boo (López-Morales & Ribas 2005). As we mentioned, the January 2010 data are reproduced by a model with one large, cold spot, which reaches the polar region of the secondary.

One should keep in mind that usually the spot temperature factor T_{spot}/T_{star} is degenerate with the spot's angular radius. This is also the case for ASAS-09. Also, none of the SAAO data sets for ASAS-09 covers both eclipses. Thus the synthetic curves plotted in Fig. 3 for the SAAO panels should be treated with caution. They were constructed only to present how the spot pattern has been changing in time and that the observations are reproduced with the "base" model from the January 2010 data.

4.2.2. ASAS-21 – a family of solutions

The case of ASAS-21 was more complicated than ASAS-09. Firstly because of a measurable eccentricity, which manifests itself in a separation of eclipses different than $0.5P$. In these cases the zero-phase moment T_0 is defined in PHOEBE in a specific

way (for details see Paper I or Prša & Zwitter 2005) and in general does not coincide with the primary eclipse. For ASAS-21 the eclipses occur at phases 0.99968 (or −0.00032) for the primary and 0.50032 for the secondary eclipse. This deviation is not visible in Fig. 4, but is measurable in PHOEBE. It is however surprising that non-zero eccentricity exists in such a system. Secondly, the out-of-eclipse patterns for the "base" data set were more complicated and did not allow us using a single spot. We decided to construct a "base" model using the July 2009 PROMPT data, because in July we obtained the full phase coverage.

For the July set we excluded the scenario of two cold spots, whose appearance is responsible for the brightness minima around $\phi = 0.3$ and $−0.2$. On tidally locked components, the brightness minimum caused by the spot would last longer than half the orbital period. This is not the case for the minimum around $\phi = 0.3$, which seems to last for about $0.4P$. The component on which such a spot could exist would have to rotate faster than in the case of tidal locking and would not explain why the same brightness modulation is observed in every consecutive cycle. Thus we conclude that in the July data either one or both brightenings (around $\phi = 0$ and 0.5) are probably caused by a bright spot. The model of a spot in PHOEBE/WD is however somewhat simplistic, so we cannot exclude a more complicated pattern of cold, dark spots.

There are two possibilities, one that in July 2009 we observed a modulation coming from two bright spots and the other that a modulation is caused by one bright spot superimposed on sine-like variations caused by a large cold spot similar to the one from the January 2010 data of ASAS-09. We concluded that the maximum appearance of this large cold spot should occur close to phase 0 (thus brightening near 0.5) not −0.4 (brightening around 0.1), since the former configuration usually reproduced the observations better than the latter. We produced a series of solutions by putting various spots on various components. We succeeded to derive a satisfactory model for every configuration with two bright spots (four cases) and with a bright eclipsed spot on the primary component when accompanied by a cold one (on either component; two cases).

Every single model was prepared in the same way as the "base" model of ASAS-09. In order to arrive at the "base" solution of ASAS-21, we took weighted average values of the Ω-potentials, inclinations and temperatures. We used the formal errors as weights while computing the averages. As the uncertainties of the average value we adopted the maximum difference between the average value and the set possible solutions. The exception were the temperatures, for which the photometric calibration is the main source of uncertainty (the typical formal error taken from PHOEBE was at the level of 10−20 K). We believe that this approach constitutes a conservative way of accounting for systematic errors in the parameters due to an uncertain spot configuration. All single values of the potentials and inclination for all six allowable solutions are listed in Table 5 with the values adopted for the "base" model. The resulting values of parameters of the "base" model and their uncertainties were incorporated into JKTABSDIM and the absolute physical parameters were calculated. They are listed in Table 6. The errors of temperatures, M_{bol}, M_V and $V - I$, as for ASAS-09, also include the uncertainty of the absolute photometric calibration. As for ASAS-09, the distance was calculated from several bolometric corrections, but for ASAS-21 we reached the best consistency for $E(B - V) \sim 0.1–0.15$.

In Fig. 4 we show all data sets in a chronological sequence. The solution for May 2008 was acheived by adding two cold
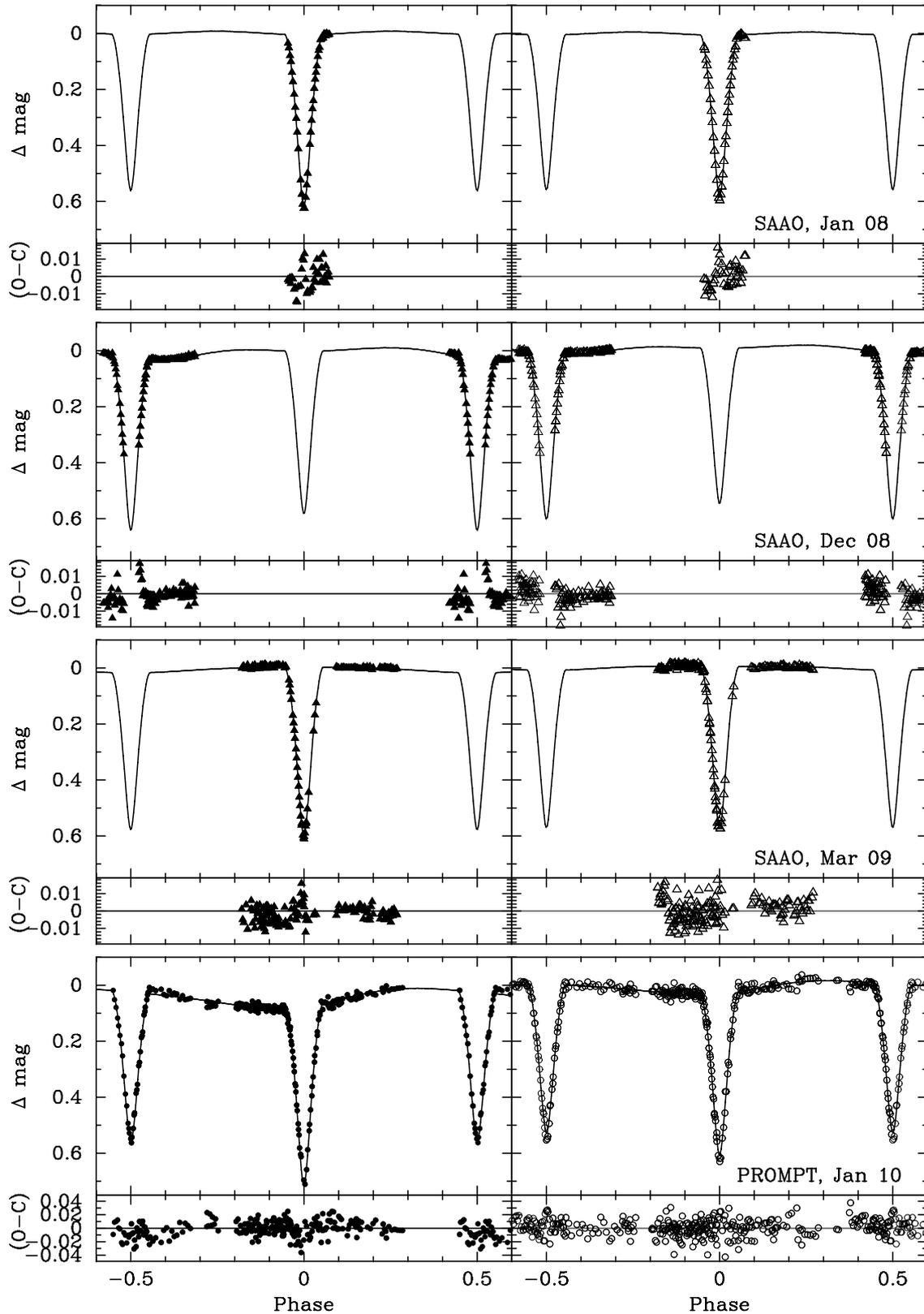
Fig. 3. The ASAS-09 light curves in the *V* (*left*, solid symbols) and *I* (*right*, open symbols) bands with their best fitting models. The SAAO data are depicted with triangles and the PROMPT data with circles. The dates of observations are given. Consecutive models differ only by the configuration of spots. The solution from January 2010 is the base one.

spots to the "base" model and by fitting for their parameters. The data from June 2009 are represented by the "base" model with two bright eclipsed spots, which is also plotted in the July panel.

These models differ from each other by the temperature factors of spots. It supports the type of the July 2009 solutions with two bright spots, since the observed differences in the brightenings
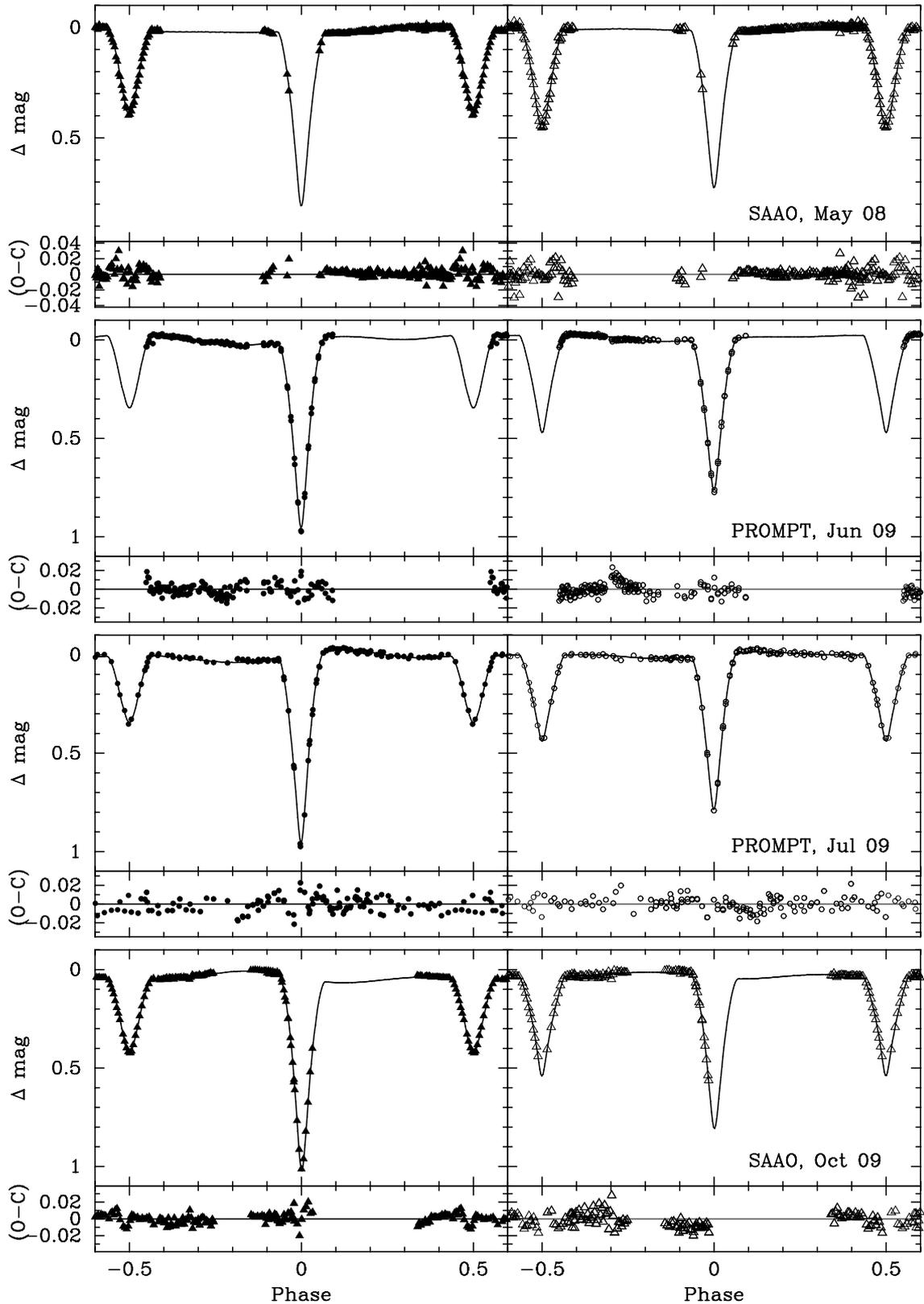
Fig. 4. The same as Fig. 3 but for ASAS-21. In this case the data from July were selected to derive a family of base solutions. Here we present an example with two bright, eclipsed spots.

levels would be hard to explain with the evolution of a large cold spot responsible either for the brightening near $\phi = 0.1$ or especially, 0.5. However, we did not exclude the latter in our aforementioned calculations in order not to underestimate the uncertainties. We also estimate that the typical time scale of spot evolution in the ASAS-21 system is about three weeks. For the remaining data set – October 2009 – we also show a model with two bright spots. A spot on the primary is responsible for the

Table 5. Potentials and inclination angle for the six solutions for ASAS-21 each with a different spot configuration.

No.	Config.	Ω_1	$\pm$	Ω_2	$\pm$	i [°]	$\pm$
1	2bn-1bn	5.365	0.039	5.496	0.027	88.66	0.7
2	1be-1bn	5.290	0.051	5.587	0.058	87.43	0.4
3	1be-2be	5.434	0.041	5.705	0.048	87.29	0.3
4	2bn-2be	5.409	0.037	5.533	0.045	87.39	0.7
5	1be-1c	5.333	0.067	5.617	0.070	88.17	0.8
6	1be-2c	5.316	0.041	5.707	0.051	86.99	0.3
	Adopted	5.368	0.078	5.572	0.135	87.35	1.31

Notes. The last line is for the weighted averages and their uncertainties adopted for the base solution of ASAS-21. The name of the configuration encodes the character and localization of the spots. The first part (3 characters) describes the spot responsible for the brightening around $\phi \sim 0.1$ and the second (2 or 3 characters) – for the maximum around $\phi \sim 0.5$. Digit "1" means the spot is on the primary, and "2" – on the secondary; "b" stands for bright spots, "c" for cold; "e" stands for an eclipsed spot, "n" for non-eclipsed (visible during an eclipse).

brightening around $\phi = -0.2$, thus it is eclipsed. It is possible that the October pattern emerged from the July one and the spots moved in longitude, but the possibility of changing the location on a tidally locked component is disputable. Again, in cases where a certain eclipse is not covered by the data, one should treat the synthetic light curve with a bit of caution.

5. Chromospheric activity

5.1. X-ray emission

The presence of stellar spots on the surface of both systems' components bears testimony to their substantial level of magnetic activity. This can be also indicated by the X-ray emission, or the X-ray-to-bolometric luminosity ratio L_X/L_{bol}. Both systems appear in the ROSAT All-Sky Bright Source Catalogue (1RXS; Voges et al. 1999) with the observed total fluxes of $0.396 \pm 0.062 \times 10^{-12}$ erg cm^{-2} s^{-1} and $0.714 \pm 0.102 \times 10^{-12}$ erg cm^{-2} s^{-1} for ASAS-09 and ASAS-21 respectively, which gives $L_X = 1.08 \pm 0.21 \times 10^{30}$ erg s^{-1} and $L_X = 1.36 \pm 0.23 \times 10^{30}$ erg s^{-1} for the distances from Tables 4 and 6.

The high level of activity is claimed to be driven by the stellar rotation. For single stars the magnetic activity has been found to be correlated with stellar rotation (Fleming et al. 1989; Bouvier 1990), but no such correlation has been found for binaries (Fleming et al. 1989), which are usually faster rotators. However, Delfosse et al. (1998) have proven that for the field M dwarfs, L_X/L_{bol} saturates already at $v_{rot} \sin i > 5$ km s^{-1}, so most of the low-mass DEBs should fall into the saturated X-ray regime where no correlation between activity and rotation exists. The general fact is that fast rotators, like tidally locked short-period binaries, show a higher level of X-ray emission than slowly rotating stars of the same mass.

López-Morales (2007) has found a clear correlation for low-mass stars between L_X/L_{bol} and the observed radii excess defined as $\Delta R = (R_{obs} - R_{mod})/R_{mod}$, where R_{obs} and R_{mod} are respectively an observed radius and a radius of a star of given mass theoretically predicted by the evolutionary models of Baraffe et al. (1998). The inflated radii of components of late-type binaries are their main characteristic and are observed for many years (see Fig. 1 in Lacy 1977). Recently, some successful efforts of an explanation involving the influence of rotationally driven magnetic activity on the effectiveness of convection and mixing have

Table 6. Absolute physical parameters adopted for ASAS-21.

ASAS-21	Primary		Secondary	
Parameter	Value	$\pm$	Value	$\pm$
inclination [°]	87.4 ± 1.3			
a [$R_\odot$]	3.838 ± 0.023			
Mass [$M_\odot$]	0.833	0.017	0.703	0.013
Ω-potential	5.368	0.078	5.572	0.135
Radius [$R_\odot$]	0.845	0.012	0.718	0.017
$\log g$	4.506	0.012	4.574	0.020
v_{synch} [km s^{-1}]	60.8	0.5	51.7	0.9
$V - I$ [mag]	1.15	0.21	1.39	0.30
T_{eff} [K]	4750	150	4220	180
M_{bol} [mag]	5.96	0.15	6.85	0.19
M_V [mag]	6.35	0.14	7.65	0.21
distance [pc]	126 ± 8			

been made and seem to have strong support in the recent burst in the number of discovered and characterized low-mass eclipsing binaries. This also includes a $P = 8.43$ d system T-Lyr1-17236, which even if rotationally synchronized should exhibit relatively low rotational velocity which therefore should not induce a high level of activity (Devor et al. 2008). However, the authors did not find a conclusive evidence for the non-activity of this system, especially considering the signatures of H$_\alpha$ emission and the 0.1 mag level of the photometric data scatter. Most of the spotted systems – including ASAS-09 and -21 – show out-of-eclipse modulation of this level or lower (see Fig. 6).

In Table 7 we present our estimates of L_X/L_{bol} based on our measurements of the radii and bolometric luminosity, radii theoretically predicted by $t = 1$ Gyr $Z = 0.02$ isochrone of Baraffe et al. (1998), and three assumptions about the X-ray luminosity and rotational velocity considered in López-Morales (2007): none, linear and quadratic correlation. In the first case (no correlation) we followed the assumption that the X-ray emission is divided equally between components. The values suggest that ASAS-21 is the more active of the two systems. We see that both systems exhibit radii inflated by about 10–12%, while their X-ray emission rates are substantially different, including the given errors. This can be explained only if no correlation between L_X and v_{rot} exists and the X-ray emission is not equally divided between the components of one system. It is also very likely that the level of X-ray emission, and thus the magnetic activity, varies in time and is not dependent on the stellar mass, at least in rapidly rotating, tidally locked binaries. This claim seems to be supported by the ASAS-09 and -21 light curves, with the out-of-eclipse modulation pattern varying in time. However, no secure conclusions can be made from our data only. An intriguing question would be whether the radii change with the varying activity level. In order to answer this question one could combine simultaneous time series of X-ray and multi-band photometric observations, preferably also with high-precision RV measurements. To the best of our knowledge, no such efforts have been carried out.

5.2. H$_\alpha$ emission

One of the most important spectral indicators of chromospheric activity is the emission in the Balmer H$_\alpha$ line. Many known low-mass stars exhibit such an emission, which is often variable and decreases in time for single stars (Hawley et al. 1999). Our low-SNR spectra make the H$_\alpha$ line identification quite challenging and impossible in the case of other activity indicating spectral

Table 7. Observed and theoretically predicted radii of ASAS-09 and ASAS-21 components and their L_X/L_{bol} calculated from the values from Tables 4 and 6 and under assumption of no, linear and quadratic correlation between L_X and v_{rot}. The numbers in parenthesis show the uncertainty.

Component	R_{obs} $[R_\odot]$	R_{mod} $[R_\odot]$	ΔR [%]	$L_X/L_{bol} \times 10^4$ ($\not\propto v_{rot}$)	($\propto v_{rot}$)	($\propto v_{rot}^2$)
ASAS-09 A	0.772(12)	0.699(28)	10.4(6.4)	7.27(31)	7.27(31)	7.28(30)
ASAS-09 B	0.769(13)	0.696(18)	10.5(4.8)	7.33(33)	7.33(33)	7.32(33)
ASAS-21 A	0.847(12)	0.751(15)	12.8(3.9)	5.40(28)	5.79(27)	6.19(26)
ASAS-21 B	0.718(17)	0.646(10)	11.1(4.5)	12.36(29)	11.45(30)	10.55(32)

emission lines. H_β was in the range of AAT/UCLES only but no conclusive identification was made. The Ca II H, K, and helium 4027 and 4473 Å lines were out of the range of both spectrographs with our setup.

In two of our AAT/UCLES spectra of ASAS-09 we identified the H_α emission line of both components, but we could make reliable measurements only of the one taken at HJD = 2 454 837.2062. We found the equivalent widths to be 0.25±0.15 and 0.15 ± 0.1 Å for the primary and secondary, respectively. The impossibility of obtaining reliable measurements in this case does not allow us to draw conclusions about the variability of the H_α emission line. However, we cannot rule it out.

We found H_α to be in emission for ASAS-21 in several Radcliffe/GIRAFFE and AAT/UCLES spectra. In the former case the line was close to the edge of an échelle order, so no meaningful measurements could be done. Emission from the primary was certain but undetectable for the secondary. This may mean however that the absorption feature of H_α was filled-in to the level of continuum. In one of the AAT/UCLES spectra we found an emission from both components with the equivalent widths of 0.4 ± 0.1 and 0.5 ± 0.1 Å for the primary and secondary respectively. From the comparison with the SAAO spectra we may conclude that at least for the secondary the H_α emission varies.

5.3. Stellar spots and their evolution

Considering the "base" model of ASAS-09 we see that probably only one component was heavily spotted at the time of observations. From the model of the spot, we deduce that the polar region of the secondary is covered. The existence of these features is not straightforward to deduce and understand. The first theoretical predictions of these features were done by Schüssler & Solanki (1992) according to whom polar spots in rapidly rotating stars are caused by the Coriolis force that overpowers the buoyancy. They can be used to explain sine-like modulations because an equatorial spot is not visible at certain phases and therefore would not modify the "clean" light curve. These sine-like modulations and polar spots were noted for low-mass CM Dra (Lacy 1977), LP 133-373 (Vaccaro et al. 2007), BD -22 5866 (Shkolnik et al. 2008), NSVS 02502726 (Çakırlı et al. 2009), ASAS J082552-1622.8 (Paper II) or a 1.13 + 1.05 $M_\odot$ binary UV Leo, (Mikuz et al. 2002; Prša & Zwitter 2005). Further photometric investigations of this system revealed that the spot pattern also had changed on a time scale of single weeks (compare Kjurkchieva & Marchev 2007; with Heckert 2009). It is also noticeable that different studies resulted in different values of the ratio of radii (see Heckert 2009). Another example of short-scale spot variations is probably a 1.38 + 1.3 $M_\odot$ pre-main-sequence binary ASAS J052821+0338.5 (Stempels et al. 2008), where the authors report significant changes in the light curve during a 110-day monitoring. A longer term evolution on time scales

of single years is reported for detached BD -22 5866 (Shkolnik et al. 2008) and RS CVn (Rodonó & Cutispoto 1994), and semi-detached ES Cnc (Pribulla et al. 2008) and RT Lac (Çakırlı et al. 2003). The variability on time scales of several hundreds of days is also seen in the cases of ASAS-09 and ASAS-21. Their long-cadence ASAS light curves exhibit semi-periodic variations with $P \sim 1000$ and 1600 d, respectively.

All this suggests that a rapid and long-time spot evolution is as common for active binaries as it is for single stars. This influences the derived properties, in particular the radii and inclination, as was shown in a recent study of GU Boo by Windmiller et al. (2010). They analyzed their new multi-band CCD and photoelectric measurements, reanalyzed photometric data of López-Morales & Ribas (2005), and found that the varying spot pattern implies a discrepancy of about 2% between the three data sets they used. Also changing the spot configuration (moving a spot from the primary to the secondary for instance) for the same data set (from López-Morales & Ribas 2005) may change the resulting radii by over 3% and the masses by 2%. We hold that this was not the case at least for ASAS-09, because a different spot configuration would lead to less probable values of the temperatures. As for ASAS-21, averaging over several models already led to ~2% uncertainties. It is an open question whether the discrepancies in radii, like those found by Windmiller et al. (2010) are caused only by the models of spots that were used or are a real manifestation of the varying level of activity. The latter however should not influence the orbital inclination, and following from this, the masses. If the variation in radii is real, it should not be at the level higher than about 1–2%, which would be difficult to detect in the case of binaries described here. To observe it, one would require a series of determinations of the component radii with about 0.5% precision from the data gathered during several observing epochs. As pointed out by Windmiller et al. (2010), there is a clear need of long-term monitoring and derivation of the absolute parameters of active systems in order to reach a better understanding of their nature.

5.4. Influence of spots on the precision

Stellar spots on rapidly rotating stars also influence the measured radial velocities. Because the spot pattern varies over single weeks, the RV and photometric observations should be done nearly simultaneously, which is not the case in our study. The RV measurements of ASAS-09 at the AAT/UCLES were carried out after about a month from the SAAO observing run in December 2008, but the December 2008 light curve is far from complete and provides no strong constrains of the configuration of spots. For this reason we did not perform our RV fits with the spots (as is possible in PHOEBE), but only checked which impact this could possibly have on the RV analysis and the derived parameter precision.
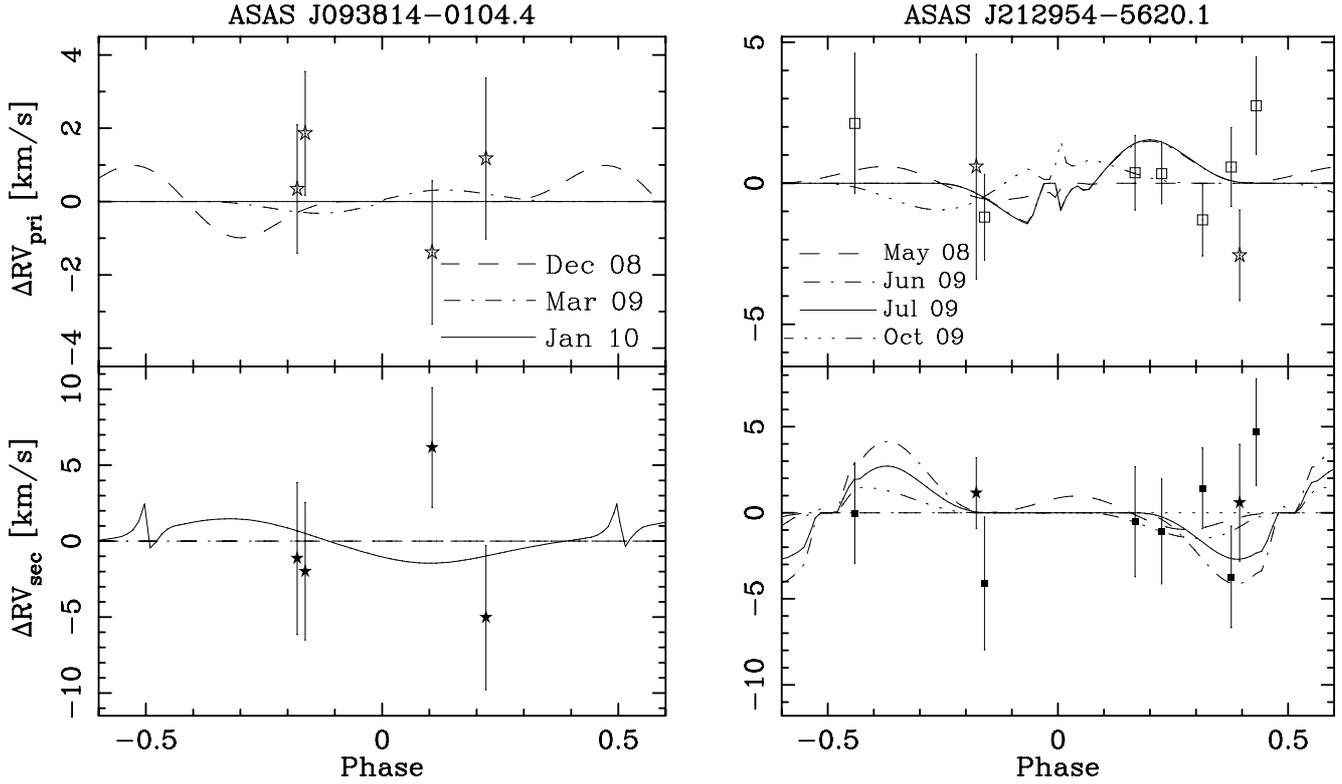
Fig. 5. Influence of stellar spots included in our model on the radial velocity curve of the primary (*top*) and secondary (*bottom*) components of ASAS-09 (*left*) and ASAS-21 (*right*) systems. ASAS-09 models were constructed with one spot and ASAS-21 with two spots (one on each component). Solid lines depict the base solution which in the case of ASAS-21 is represented by the configuration, with two eclipsed spots. Points with errorbars are the residua of the orbital fit. Their coding is the same as in Fig. 2.

We show the spot-originated RV modulation in Fig. 5 and the influence on the light curves from the models in Fig. 6. The differential RV curves for the primary component are shown in the upper panels and for the secondary components in the lower ones. The base solutions are depicted with solid lines. The ΔRV curves are compared with the orbital fit residuals and errorbars. The point coding is the same as in Fig. 2. For ASAS-09 we can see no differences in the RVs either, because our models were constructed with only one spot on a certain component.

For ASAS-21 the bright (eclipsed) spot on the primary for the June solution is very similar to the analogical spot from the July model (with two eclipsed spots), so not much of a difference is seen between those cases of ΔRV for the primary nor of ΔV or ΔI around $\phi \sim 0.1$ (Fig. 6). An evolution of the spot on the secondary is obvious however and in our opinion the scenario of two bright spots in the system is the best one to explain this behavior in a simple way. Figure 6 shows that at longer wavelengths (I band) the influence is much smaller, thus RVs measured near-IR should not be significantly affected by the spots (as confirmed for example by Figueira et al. 2010). It also means that spectrographs with a long spectral range will produce RV measurements with larger errors if the spot information is excluded from the analysis. It would be presumably possible to find a correlation between the échelle spectrum order numbers (e.g. their central wavelength) and RV measurements from single orders, which would enable us deduce some information about the spot itself. It is also worth noting how the presence of a cold spot on the secondary component of ASAS-09 in the January 2010 model makes the primary eclipse deeper.

From Fig. 5 we can see that the RV errorbars and their spread is bigger than the possible influence of spots. We can conclude therefore that the condition of obtaining χ^2 of the orbital fit equal to 1, mainly through adding a systematic term, is sufficient to compensate for the influence of stellar activity. This was already shown in Paper II. We believe that the uncertainties of the derived parameters given in Tables 4 and 6 are well estimated and reliable even though that the spectroscopic and photometric observations were not carried out simultaneously and the spot pattern has changed. Likely obtaining all data at (nearly) the same time would allow for a better precision of the results.

6. Age estimate and evolutionary status

6.1. Kinematics

We calculated the galactic velocities U, V, and W[3] with regard to the local standard of rest (LSR, Johnson & Soderblom 1987). We took our values of distance and systemic velocity (with uncertainties, and assuming $\gamma_1 - \gamma_2 = 0$), and applied the positions and proper motion values from the UCAC3 (Zacharias et al. 2010). We obtained $U = -4.5 \pm 2.9$, $V = -21.0 \pm 3.0$, and $W = 4.5 \pm 3.1$ km s^{-1} for ASAS-09, which puts it definitely in the young disk, at the edge of a region occupied in the (U, V, W) space by the Pleiades moving group (PMG, a.k.a. the Local Association; Seabroke & Gilmore 2007; Zhao et al. 2009). The PMG is claimed to be between 20 and 150 Myr old (Montes et al. 2001) with a metal abundance bellow solar (Zhao et al. 2009).

---

[3] Positive values of U, V and W indicate velocities toward the Galactic center, direction of rotation and north pole respectively.
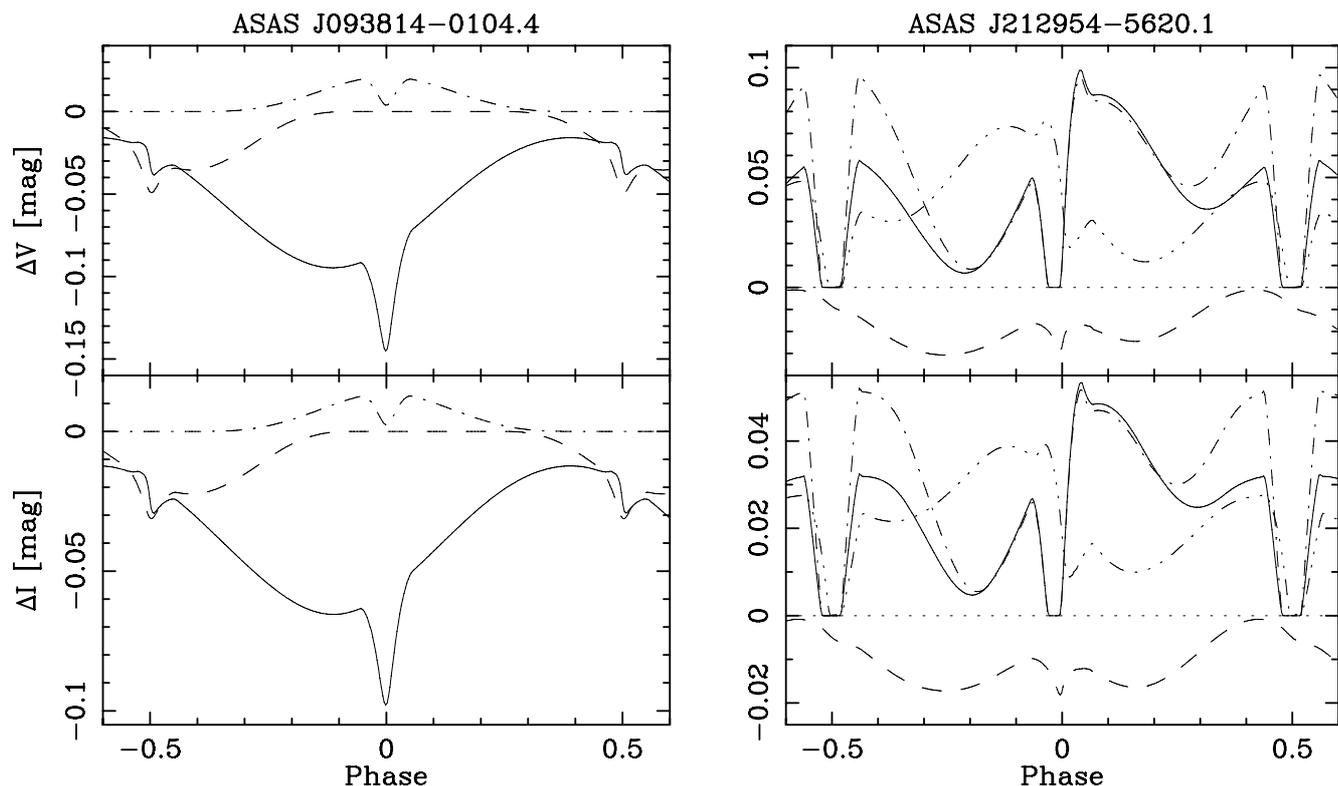
Fig. 6. Influence of stellar spots included in our model on the *V* (*top*) and *I* band (*bottom*) light curves of ASAS-09 (*left*) and ASAS-21 (*right*) systems. The line encoding is the same as in Fig. 5. For the purpose of clarity the zero-level is shown at ASAS-21 plots only with a dotted line.

The values of galactic velocities we obtained for ASAS-21 – $U = -40.6 \pm 2.6$, $V = -56.1 \pm 4.0$ and $W = 4.3 \pm 1.1$ km s^{-1} – put this system kinematically in the so called Hercules Stream (Seabroke & Gilmore 2007; Zhao et al. 2009). This feature is a mixture of young and old stars, which show kinematic characteristics typical for the thick galactic disk (Bensby et al. 2007). If so, the ASAS-21 system can be as old as 8 Gyr (lower limit for the thick disk age, Jimenez et al. 1998) or more. Considering the kinematics, ASAS-21 appears to be older than ASAS-09. However, the measured excess in radii and the L_X/L_{bol} ratio (Table 7) suggest that it is more active than ASAS-09. This is possibly connected to the smaller separation and the fact that the secondary of ASAS-21 is less massive than the ASAS-09 components, which for single stars would directly mean a higher level of activity. A smaller separation also indicates higher rotational velocities, which in turn may additionally increase the activity level of both components, if such a correlation still exists for high v_{rot}.

6.2. Isochrones

We compare our results with several popular and widely used sets of theoretical evolutionary models. For our purposes we chose Y^2 (Yi et al. 2001; Demarque et al. 2004), BCAH98 (Baraffe et al. 1998), PADOVA (Girardi et al. 2000; Marigo et al. 2008) and GENEVA (Lejeune & Shaerer 2001). In Fig. 7 we show our measurements in the mass M vs. (from top to bottom) the bolometric luminosity M_{bol}, radius R, logarithm of the effective temperature $\log T_{eff}$, absolute V magnitude M_V, and $V - I$ color. ASAS-09 is the close pair near $M = 0.77$ $M_\odot$. In order to show the probable properties of the researched systems, we made our comparison for three cases: (1) for nearly-solar metallicity $Z = 0.02$ and age $t = 1$ Gyr; (2) for $Z = 0.02$ and $t = 5$ Gyr; (3) $t = 1$ Gyr and metal abundance above solar, which varies de-

pending on the set of isochrones: 0.03 for PADOVA, and 0.04 for Y^2 and GENEVA. The last one is defined only to $M = 0.8$ $M_\odot$, but it is reasonably close to our mass determinations to make an attempt at extrapolation. Because the BCAH98 set is not available for metallicities above solar, we show the isochrone for $Z = 0.02$, but with $Y = 0.282$ (normally 0.275 or 0.25), since it fits within errors to our measurements of M_{bol} for both systems.

We consider the M/M_{bol} as the most important figure because theoretical models seem to reproduce this combination of parameters properly for low-mass eclipsing binaries. For the ASAS-09 system we also gave more attention to the $M/(V - I)$ panel because in the distance determination we found $E(B-V)$ in this direction close to 0 and the uncertainty coming from dereddening is negligible. Our values of $V - I$ derived from PHOEBE are nearly equal for both components, as expected for twin stars. Thus they represent the color of the entire system. Our result – 1.17 ± 0.13 mag – agrees well with 1.12 from Szczygieł et al. (2008).

We see that the bolometric luminosity of ASAS-09 is within errors in agreement with every theoretical model presented. We also observe a situation typical for most of these systems – the radii are larger and temperatures lower than predicted. The isochrone that is closest either in $M/\log T_{eff}$ or M/R plane is the BCAH98 for $Y = 0.282$ and $t = 1$ Gyr. This case fits our measurements best. All models for $Z > 0.02$ and $t = 1$ Gyr agree within errors not only with the system's M_{bol} and $V - I$, but also with M_V, which is not the case for models with $Z = 0.02$. Thus we may suspect that ASAS-09 is a main-sequence, metal-enriched and/or helium-depleted system, probably nearly 1 Gyr old. We should also note that a lower metallicity results in a higher bolometric luminosity. Hence no $Z < 0.02$ isochrone fits to ASAS-09 regardless of the age. This constitutes an argument against the membership of ASAS-09 in the Pleiades moving group.
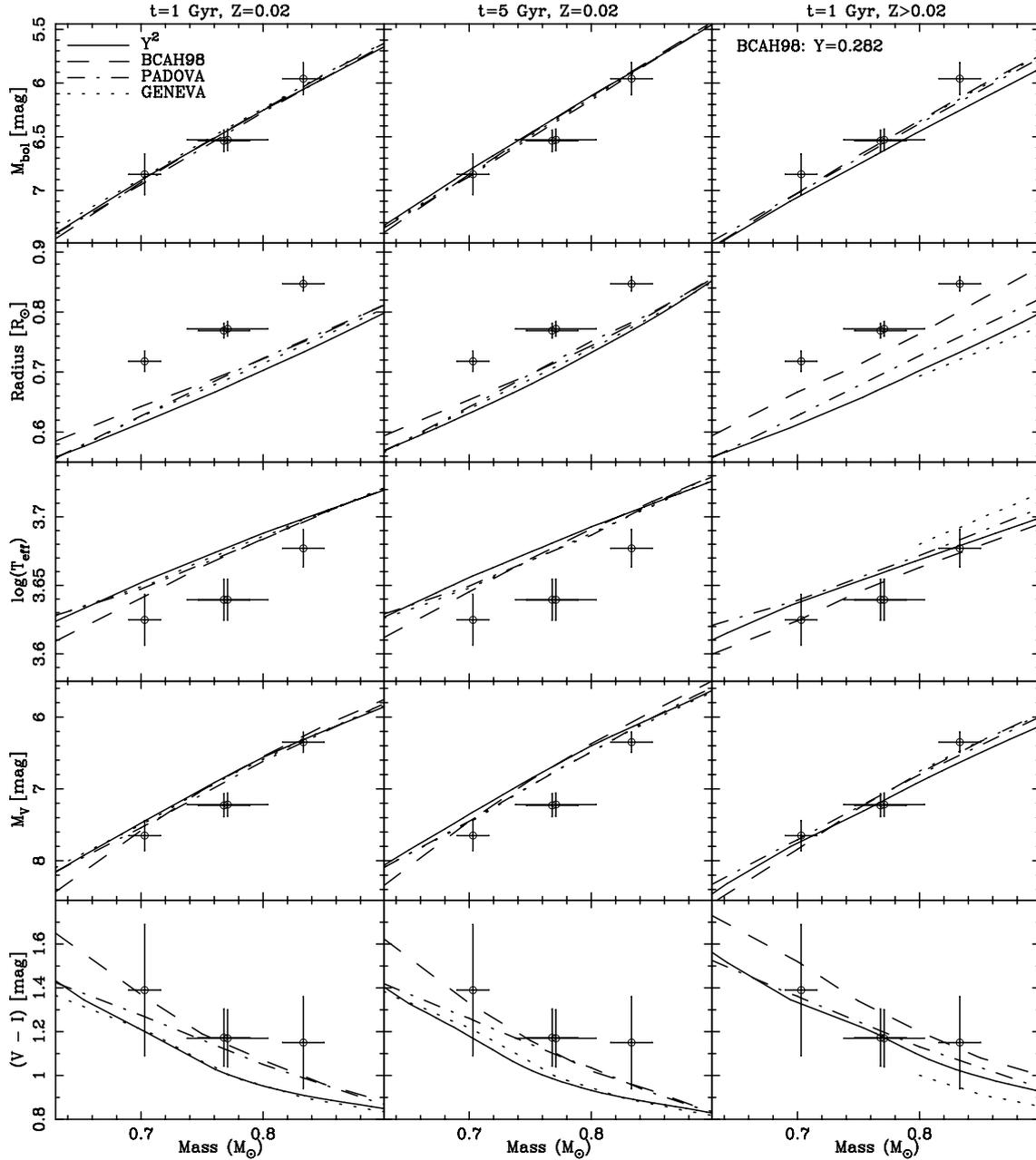
Fig. 7. Comparison of various parameters as a function of mass for ASAS-09 (inner pair) and ASAS-21 with several sets of isochrones. *Left column* is for the age of 1 Gyr and nearly-solar metallicity, *middle column* is for 5 Gyr and $Z = 0.02$, *right column* is for 1 Gyr and metal-enriched composition: 0.03 for PADOVA, and 0.04 for Y^2 and GENEVA (available for $M \geq 0.8\ M_\odot$). For the comparison we also show an isochrone of $Y = 0.282$ for BCAH98.

The situation is slightly different for ASAS-21. The absolute V magnitude is best reproduced in the $t = 1$ Gyr, $Z = 0.02$ case. However, in other M/M_V panels the models still agree with the measurements. The best M_{bol} fit is obtained for the 5 Gyr case and the worst one for metal-enriched models. On the other hand, $Z > 0.02$ models reproduce temperatures but, as mentioned before, it would be an unusual case for a low-mass eclipsing binary, and this panel is shown only for comparison. Thus ASAS-21 has a metal abundance similar to solar and is likely on the main sequence, but closer to 5 Gyr than to 1 Gyr, as suggested by the kinematics and the M/M_{bol} plane. It is possible that ASAS-21 is a member of the Hercules Stream. The marginal discrepancy in the $V - I$ color (for two models only) may come from the uncertainty in $E(B - V)$ estimate and the system is slightly bluer.

7. Conclusions

We presented the results of the analysis of two newly discovered spectroscopic double-lined low-mass eclipsing binaries – ASAS J093814-0104.4 and ASAS J212954-5620.1 – found by us through the spectroscopic survey for low-mass systems from the ASAS catalogue. We did not succeed in reaching the desired 3% precision only in the mass of ASAS-09. However, we are reasonably sure that for these two objects it is possible to reach a sub-% level of precision in the absolute values of physical parameters with more spectroscopic and photometric data. We also estimate the scale of the influence of stellar activity on the parameters and find that this effect is most likely already compensated. The configuration of stellar spots in both systems changes

on time scales of single weeks, which is a manifestation of a substantial level of activity – their main characteristic. The evolution of spots is a known feature of active stars, but such a rapid one was not previously reported for low-mass eclipsing system (see Sect. 5.3) and rarely reported in general. The variability of spots is a major obstacle in an analysis of binary systems such as ASAS-09 and ASAS-21. In order to make the best-fitting parameters more precise, one should ideally make nearly simultaneous spectroscopic and photometric observations, at least for short period binaries like ASAS-09 and ASAS-21, to properly account for the influence of spots on the RV curve.

As pointed out by Windmiller et al. (2010), in order to properly characterize and understand the properties of many active systems, several separate observing programs would be required. This would for example allow one to estimate the spread of measured radii and temperatures and possibly correlate it with the level of activity (Windmiller et al. 2010) and/or eventually evaluate how the derived radii and temperatures change with the configuration of spots, H_α emission, or other activity indicators. A more intensive monitoring of known active eclipsing binaries is also required to find more systems exhibiting an evolution of spots on various time scales.

Considering the above, we admit that parameters of ASAS-09 and ASAS-21 can be certainly improved and in our opinion these systems deserve more attention. We do not know many "stellar twins", like ASAS-09, among all known eclipsing systems, and untill now only three other low-mass eclipsing systems were found. The high-precision derivations of their parameters can serve as a critical test for the validity of the Vogt theorem. This theorem says that stars of the same chemical composition have their radii, temperatures, and bolometric luminosities strictly determined by their masses (Vogt 1926). Despite a wide (but controversial) criticism of this theorem, it is still the basis of the stellar evolution theory and is taken for granted. No reliable empirical tests of this theorem have been made (for a brief discussion and references see: Lastennet & Valls-Gabaud 2002). Eclipsing "twins", very accurately characterized, should be perfect targets for such a research. In the case of active systems the radii and temperatures may be (and probably are) affected by the likely different level of activity of the components, but their M_{bol} should not. A more extensive study of these systems such as YY Gem or ASAS-09 should validate the Vogt theorem at least at a certain level.

Owing to its relatively low mass ratio, ASAS-21 is particularly interesting for testing evolutionary models. Systems with low q provide much more stringent tests than binaries with nearly equal masses, and the parameters derived from the fitting of isochrones (if successful) are more accurate. The value of q obtained for ASAS-21 is lower than for most of the known double-lined binaries (Lucy 2006) and one of the lowest among late-type eclipsing systems. There is an additional difficulty in finding low-q binaries, which is the low brightness ratio of the binary components. The identification of the faint lines of the secondary or the shallow secondary eclipse is then challenging and requires high SNR data (for an extreme case of eclipse depths see Maceroni et al. 2009). Considering that, any new object with $q \lesssim 0.85$ is valuable.

References

Baraffe, I., Chabrier, G., Allard, F., & Hauschildt, P. H. 1998, A&A, 337, 403
Bessel, M. S., Castelli, F., & Plez, B. 1998, A&A, 333, 231
Bensby, T., Oey, M. S., Feltzing, S., & Gustafsson, B. 2007, ApJ, 655, L89
Blake, C. H., Torres, G., Bloom, J. S., & Gaudi, B. S. 2008, ApJ, 684, 635
Bopp, B. W. 1974, ApJ, 193, 389
Bouvier, J. 1990, AJ, 99, 946
Casagrande, L., Portinari, L., & Flynn, C. 2006, MNRAS, 373, 13
Castelli, F., & Kurucz, R. 2003, IAUS, 210, A20 [arXiv:astro-ph/0405087v1]
Çakırlı, Ö., İbanoğlu, C., Djurašević, G., et al. 2003, A&A, 405, 733
Çakırlı, Ö., İbanoğlu, C., & Güngör, C. 2009, NewA, 14, 496
Chabrier, G., Gallardo, J., & Baraffe, I. 2007, A&A, 472, L17
Clausen, J. V. 2008, A&A, 487, 1095
Creevey, O. L., Benedict, G. F., Brown, T. M., et al. 2005, ApJ, 625, L127
Cutri, R. M., Skrutskie, M. F., Van Dyk, S., et al. 2003, The 2MASS All-Sky Catalog of Point Sources, University of Massachusetts and Infrared Processing and Analysis Center (IPAC/California Institute of Technology)
Delfosse, X., Forveille, T., Perrier, C., & Mayor, M. 1989, A&A, 331, 581
Delfosse, X., Forveille, T., Mayor, M., Burnet, M., & Perrier, C. 1999, A&A, 341, L63
Demarque, P., Woo, J.-H., Kim, Y.-C., & Yi, S. K. 2004, ApJS, 155, 667
Devor, J., Charbonneau, D., Torres, G., et al. 2008, ApJ, 687, 1253
Diaz-Cordovez, J., & Gimenez, A. 1992, A&A, 259, 227
Etzel, P. B. 1981, Photometric and Spectroscopic Binary Systems, 111
Figueira, P., Pepe, F., Melo, C. H. F., et al. 2010, A&A, 511, 55
Fleming, T. A., Gioia, I. M., & Maccacaro, T. 1989, ApJ, 340, 1011
Flower, P. J. 1996, ApJ, 469, 355
Girardi, L., Bressan, A., Bertelli, G., & Chiosi, C. 2000, A&AS, 141, 371
Girardi, L., Bertelli, G., Bressan, A., et al. 2002, A&A, 391, 195
Halbwachs, J. L., Mayor, M., Udry, S., & Arenou, F. 2003, A&A, 397, 159
Hawley, S. L., Reid, I. N., & Tourtellot, J. G., 1999, in Solar and Stellar Activity: Similarities and Differences, ed. C. J. Butker, & J. G. Doyle (San Francisco: ASP), ASP Conf. Ser., 158, 63
Heckert, P. A. 2009, IBVS, 5912, 1
Hełminiak, K. G., & Konacki, M. 2010, A&A, 526, A29 (Paper II)
Hełminiak, K. G., Konacki, M., Ratajczak, M., & Muterspaugh, M. W. 2009, MNRAS, 400, 969 (Paper I)
Jimenez, R., Flynn, C., & Kotoneva, E. 1998, MNRAS, 299, 515
Johnson, D. R. H., & Soderblom, D. R. 1987, AJ, 93, 864
Kjurkchieva, D. P., & Marchev, D. V. 2007, MNRAS, 381, 663
Kron, G. E. 1952, ApJ, 115, 301
Lastennet, E., & Valls-Gabaud, D. 2002, A&A, 396, 551
Lacy, C. H. 1977, ApJ, 218, 444
Landolt, A. U. 1992, AJ, 104, 340
Lejeune, T., & Shaerer, D. 2001, A&A, 366, 538
López-Morales, M. 2007, ApJ, 660, 732
López-Morales, M., & Ribas, I. 2005, ApJ, 631, 1120
Lucy, L. B. 1967, ZAp, 6, 89
Lucy, L. B. 2006, A&A, 457, 629
Maceroni, C., Montalbán, J., Michel, E., et al. 2009, A&A, 508, 1375
Marigo, P., Girardi, L., Bressan, A., et al. 2008, A&A, 482, 883
Mikuz, H., Dintinjana, B., Prša, A., Munari, U., & Zwitter, T. 2002, IBVS, 5338, 1

Montes, D., López-Santiago, J., Gálvez, M. C., et al. 2001, MNRAS, 328, 45
Morales, J. C., Torres, G., Marschall, L. A., & Brehm, W. 2009, ApJ, 707, 671
Pojmański, G. 2002, Acta Astron., 52, 397
Popper, D. M., & Etzel, P. B. 1981, AJ, 86, 102
Pribulla, T., Rucinski, S., Matthews, J. M., et al. 2008, MNRAS, 391, 343
Prša, A., & Zwitter, T. 2005, ApJ, 628, 426
Rodonó, M., & Cutispoto, G. 1994 Mem. Soc. Astron. Italiana, 65, 83
Schüssler, M., & Solanki, S. K. 1992, A&A, 264, L13
Seabroke, G. M., & Gilmore, G. 2007, MNRAS, 380, 1348
Shkolnik, E., Liu, M. C., Reid, I. N., et al. 2008, ApJ, 682, 1248
Southworth, J., Maxted, P. F. L., & Smalley, B. 2004a, MNRAS, 351, 1277
Southworth, J., Zucker, S., Maxted, P. F. L., & Smalley, B. 2004b, MNRAS, 355, 986
Stempels, H. C., Hebb, L., Stassun, K. G., et al. 2008, A&A, 461, 747

Szczygieł, D. M., Socrates, A., Paczyński, B., Pojmański, G., & Pilecki, B. 2008, Acta Astron., 58, 405
Torres, G., & Ribas, I. 2002, ApJ, 567, 1140
Torres, G., Andersen, J., & Gimenéz, A. 2010, A&AR, 18, 67
Vaccaro, T. R., Rudkin, M., Kawka, A., et al. 2007, ApJ, 661, 1112
van Hamme, W. 1993, AJ, 106, 2096
Voges, W., Aschenbach, B., Boller, Th., et al. 1999, A&A, 349, 389
Vogt, H. 1926, Astron. Nachr., 226, 301
Wilson, R. E., & Devinney, E. J. 1971, ApJ, 166, 605
Windmiller, G., Orosz, J. A., & Etzel, P. B. 2010 ApJ, 712, 1003
Yi, S., Demarque, P., Kim, Y.-C., et al. 2001, ApJS, 136, 417
Zacharias, N., Finch, C., Girard, T., et al. 2010, AJ, 139, 2184
Zhao, J., Zhao, G., & Chen, Y. 2009, ApJ, 692, L113
Zucker, S., & Mazeh, T. 1994, ApJ, 420, 806